Check for updates

Urea-doped carbon dots as fluorescent switches for the selective detection of iodide ions and their mechanistic study†

Kai Wang, [ID] *[a] Cuihuan Geng,[a] Fang Wang,[a] Yajun Zhao[c] and Zongling Ru*[b]

A facile and green strategy for the fabrication of fluorescent urea-doped carbon dots (N-CDs) has been explored. Significantly, the fluorescent N-CDs could recognize iodide ions (I^-) with high selectivity, and their photoluminescence could be efficiently quenched by the addition of I^-. The sensitivity analysis for I^- indicated a linear relationship in the range from 12.5 to 587 μM with the detection limit as low as 0.47 μM. Furthermore, the I^- induced fluorescence (FL) quenching mechanism was investigated employing a combination of techniques, including UV-vis/fluorescence spectroscopy, Density Functional Theory (DFT) calculation, TEM and time-resolved fluorescence decay measurements. The DFT calculation results demonstrated that the amino- and amide groups of N-CDs play a significant role in iodide recognition through the formation of multiple $N–H \cdots I^-$, $C–H \cdots I^-$ and $C(=O)N–H \cdots I^-$ interactions with I^-. The TEM experiment confirmed the aggregation process when I^- was added to the N-CDs solution. Moreover, the radiative decay rate of N-CDs, which was first measured and reported the kinetic behaviors of the FL-quenching process, decreased from $3.30 \times 10^7 \text{ s}^{-1}$ to $1.95 \times 10^7 \text{ s}^{-1}$ after the coordination with I^- ions. The reduced lifetime demonstrated that the excited energy dissipation led to a dynamic quenching process. Therefore, such carbon materials can function as effective fluorescent switches for the selective detection of I^- ions.

1. Introduction

Iodide (I^-) is an important trace element that plays a crucial role in maintaining and regulating the stability of the intracellular environment in the human body.[1,2] Either deficiency or abundance of iodide can cause harm to the body and result in relevant thyroid diseases, such as goiter, hypothyroidism, and hyperthyroidism.[3–5] Thus, it is vital to develop simple and effective methods for the determination and dynamic tracking of iodide ions, which can provide abundant physiological and pathological information in clinical medicine. Until now, several approaches, such as spectrophotometry,[6] voltammetry,[7] potentiometry,[8] and chromatography, have been proposed for the detection of iodide ions.[9] However, many of the above methods are time-consuming for sample pre-treatment or difficult in realizing online real-time monitoring. Spectrofluorimetry has attracted wide attention due to its advantages of rapid response and high sensitivity. In recent years, many fluorescent sensors have been developed for the detection of iodide ions,[10] including benzimidazole derivatives,[11,12] gold (silver) nanoparticle clusters,[13,14] porphyrin derivatives,[15] graphene oxide and graphitic carbon nitride.[16,17] Unfortunately, these fluorescent sensors usually either involve complicated organic synthesis or need the help of coordination between iodide and heavy metal ions, which impede their practical applications.[10] Therefore, it is very meaningful to develop green preparation strategies for fluorescent materials that can be used for iodide detection.

Carbon dots (CDs), owing to their stable properties and good biocompatibility, have received extensive attention from scientists in the field of chemistry, material science and medical science.[18–21] Different from traditional fluorescent organic dyes and semiconductor nanocrystals, CDs exhibit excellent properties, *i.e.*, stable photoluminescence, adjustable emission, good biocompatibility and low toxicity.[22–25] CDs can be prepared from various materials, which can be grouped into two classes, namely small organic molecules and green carbon precursors, on the basis of the chosen carbon source.[26–28] Nature is a limitless source, which inspired us to develop new ideas on novel nanomaterials with excellent properties. Thus, the preparation of new CDs has been continuously explored.

It has been reported that urea or thiourea derivatives can selectively detect anions through fluorescence spectroscopy or electrochemical methods.[29,30] However, to our best knowledge,

[a]School of Chemical and Environmental Engineering, Anyang Institute of Technology, Anyang, 455000, China. E-mail: wangkevin07@163.com

[b]School of Materials Science and Engineering, Anyang Institute of Technology, Anyang, 455000, China. E-mail: hgxrzl2007@163.com

[c]Teaching and Research Office of Neihuang Country, Anyang, 456300, China

† Electronic supplementary information (ESI) available. See DOI: 10.1039/d1ra04558j

urea-modified CDs as highly efficient anion sensors and their sensing mechanism are seldom reported.[31] Cotton is one of the most abundantly available and important material resources, which can be comprehensively used.[32–34] The main component of white cotton is cellulose, which contains plenty of hydroxyl groups. Herein, considering the environmental concerns, we report a green strategy for the synthesis of highly fluorescent CDs with white cotton as the raw material and urea as the nitrogen source. More importantly, we further demonstrate that the prepared urea-doped carbon dots (N-CDs) can act as a robust fluorescent probe for the direct detection of iodide ions by the "mixing and testing" method without the need for coordination with heavy metal ions (Scheme 1).

2. Materials and methods

2.1 Materials

White cotton was provided by the Cotton Research Institute, Chinese Academy of Agricultural Sciences. $(NH_2)_2CO$, KI, KBr, KCl, KF, and quinine sulfate were purchased from Macklin Ltd.

2.2 Instruments

Transmission Electron Microscopy (TEM) images were recorded on JEM-2100F and Talos F200S at an acceleration voltage of 200 kV. FTIR spectra were acquired on a Nicolet iS10 spectrometer. The XRD spectra of the samples were measured on a Rigaku (MiniFlex) powder X-ray diffractometer with CuKα radiation ($\lambda = 0.1540$ nm). Ultraviolet-visible (UV-vis) spectra were recorded using a Shimadzu UV-3100 instrument. Fluorescence spectra (FL) were obtained with an F-7000 fluorescence spectrophotometer (Hitachi, Japan). The nanosecond fluorescence lifetime measurements were performed on a lifetime and steady-transient state spectrometer (Edinburgh Instruments FLS980) using the time-correlated single-photon counting (TCSPC) system. The samples were excited by a 370 nm picosecond diode laser (2 MHz repetition rate), and the statistics results were analyzed by reconvolution fits.

2.3. Preparation of N-CDs

To prepare the carbon dots, 0.50 g white cotton and 4.0 g urea were dissolved in deionized water (20 mL) under stirring. Afterward, the suspension was transferred to a poly(tetrafluoroethylene) autoclave (50 mL) and heated at 210 °C for 12 h. After the reaction, the reactors were cooled to room temperature using water. The crude product, which was a yellow fluorescent solution, was obtained by removing the large dots using a 0.22

μm filter membrane. The filtrate was dialyzed against distilled water through a dialysis membrane with an MWCO of 1000 Da to remove salt and impurities. After freeze-drying, the sample was kept in a dark and cool bottle for further study.

2.4 Measurement of quantum yield

Quinine sulfate (0.1 M H_2SO_4 as the solvent, $\Phi_F = 54\%$) was employed as the standard to measure the quantum yields (QYs) of N-CDs through the slope method. The QYs were calculated by comparing the integrated fluorescence intensity (excited at 360 nm) and the absorbance value (the value was below 0.1 at the excitation wavelength). The slope method equation used is as follows:

$$\Phi_x = \Phi_{st}(K_x/K_{st})(\eta_x/\eta_{st})^2$$

where Φ is the quantum yield, K is the slope of the linear fitting curves and η is the refractive index of the corresponding solvent.

2.5 Fluorescence detection of I^-

Ultrapure water was used to prepare a KI solution of 50 mM concentration; then, I^- solutions of different concentrations (12.5 μM, 37.5 μM, 87.5 μM, 187.5 μM, 287.5 μM, 387.5 μM, 587.5 μM, 887.5 μM, 1.287 mM, 1.687 mM, 2.562 mM, 4.312 mM, 6.062 mM, 7.812 mM, 9.562 mM) were separately added into the N-CDs solution (50 μg mL⁻¹, 2 mL) by diluting the above-mentioned stock solution. After incubation for 30 s, the FL emission intensity spectra were measured at 410 nm.

The FL spectra of N-CDs (50 μg mL⁻¹, 2 mL) with different halide ions (Br^-, Cl^-, F^-) were examined to estimate the selectivity of the sensing system. The concentration of various halide ions was 9.6 mM.

2.6 Density Functional Theory (DFT) calculation

All the theoretical calculations were performed using the Gaussian 09 program at the bp86/6-31G (d) level. Then, the vibrational spectrum of each molecule was calculated at the same level of theory to ensure that all the structures correspond to the true minima of the potential energy surface. Meanwhile, the lowest unoccupied molecular orbitals (LUMO) and highest occupied molecular orbitals (HOMO) were calculated, the relative energy gaps (E_{gap}) were obtained thereby. Finally, the Gibbs free energies of N-CDs, iodide ions (I^-) and N-CD/I^- in water (298.15 K) were calculated at the bp86/6-31G (d) level. Subsequently, the corresponding binding energies between N-CDs and iodide ions were obtained as well.

2.7 Determination of I^- in real samples

For the analysis of real samples, tap water was collected and pre-treated by exposing it to sunlight and heat for two hours. A standard addition method was employed to validate the proposed fluorescent switch. The procedure was the same as the above-mentioned iodide ion detection method, except that the standard I^- solutions (0, 4, 20, 60 and 100 μM) added into the N-CDs solution were replaced by the real samples.
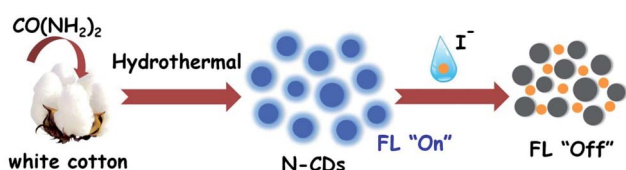
Scheme 1 The preparation of N-CDs and their application in iodide detection.

© 2021 The Author(s). Published by the Royal Society of Chemistry

3. Results and discussion

3.1 Characterization of the N-CDs

The fluorescent CDs were prepared by a one-step hydrothermal method with cotton as the precursor; the quantum yield (QY) of the cotton-based carbon dots (C-CDs) was 6.05% (Fig. S1a, ESI†). The QY of C-CDs increased with urea as the N-dopant. Upon changing the amount of doped urea from 1 equivalent to 8 equivalent, the QY of the urea-doped CDs (N-CDs) gradually increased from 7.32% to 18.79% (Fig. S1b and Table S1, ESI†). When the amount of added urea was increased again, the QY of N-CDs started to decline, which is illustrated in Table S1.† The morphologies and sizes of the N-CDs were characterized through transmission electron microscopy (TEM) (Fig. 1a, S2a and b, ESI†). The representative TEM image showed that the typical product contained a variety of N-CDs well-dispersed across the whole section, and the size statistic of the N-CDs indicated that their sizes were centered between 4–5.5 nm (Fig. 1b). However, N-CDs particles that possessed well-resolved lattice fringes were not observed in the high-resolution TEM image (inset in Fig. 1a, S2c and d, ESI†). The XRD pattern exhibited a typical intense peak centered at 24° (002 plane), which was associated with highly disordered carbon atoms (Fig. 1c).[35] The XRD pattern of the as-prepared N-CDs also displayed a weak peak at 37° corresponding to the (101) plane. The poor crystalline nature of N-CDs demonstrated the presence of more oxygen-containing functional groups on their surface.

Additionally, the surface functional groups of N-CDs were further characterized by, FTIR spectra (Fig. 1d). Broad and strong bands associated with the stretching vibrations of the C–OH and C–NH$_2$ groups were found at 3427 cm^{-1} and 3234 cm^{-1}, respectively. The peaks at 2870 cm^{-1} and 1290 cm^{-1} were assigned to the stretching vibration and bending vibration of the C–H groups, respectively. The peaks at about 1640 cm^{-1} and 1590 cm^{-1} corresponded to the stretching vibration of the carbonyl (C=O) groups. Besides, the absorption bands ranging from 1250 to 1000 cm^{-1} were attributed to a large number of C–O–C groups. The N–H deformation vibration was observed at 800 cm^{-1}.[36] Consequently, the N-CDs are hydrophilic and stable in aqueous solutions because of a large number of hydroxyl-, amino- and amide groups on the surface.

3.2 Optical properties of N-CDs

The UV-vis absorption spectrum showed that the prepared C-CDs had a broad peak around 325 nm, while the N-CDs solution exhibited a broad absorption band centered at 275 nm, which was ascribed to the n–π* transition of the C=O bonds or C=C–NH$_2$ groups (Fig. 2a).[37,38] This blue-shift phenomenon was due to the introduction of amino- and amide groups on the surface of N-CDs. The as-prepared solution of N-CDs was yellow under visible light, while it showed blue color under UV light (365 nm), which exhibited their blue photoluminescence property (inset in Fig. 2b). As shown in Fig. 2b, the maximum emission wavelength of N-CDs in water red-shifted gradually
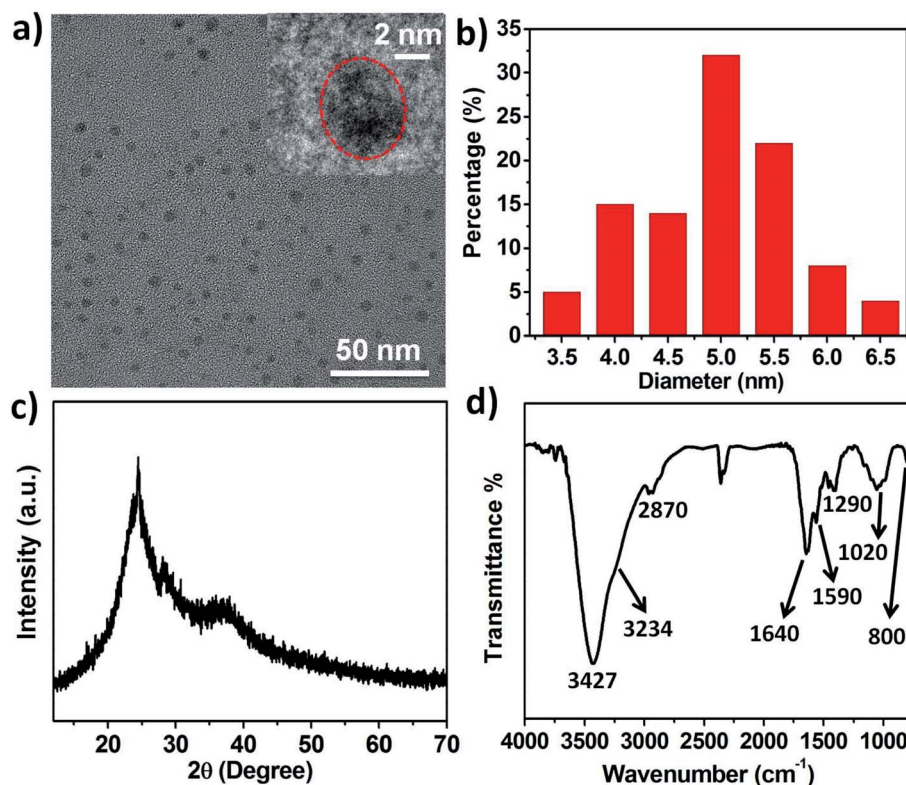

Fig. 1 (a) TEM image of the prepared N-CDs. Inset: the high-resolution TEM image of N-CDs. (b) The size distribution histogram of N-CDs. (c) XRD pattern of N-CDs. (d) FTIR of N-CDs.
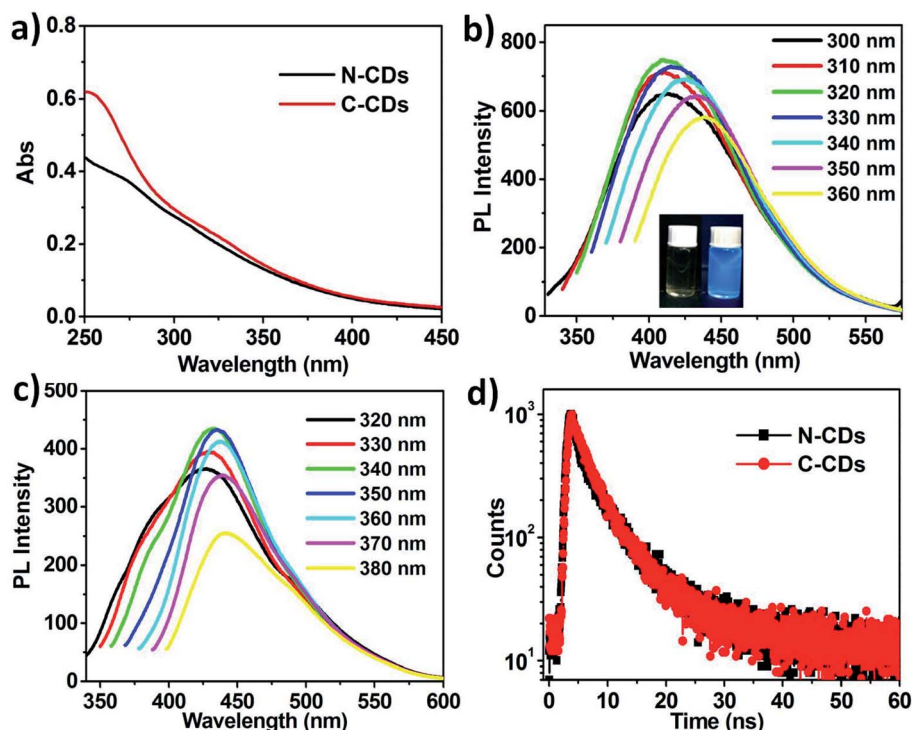
Fig. 2 (a) UV-vis absorption of N-CDs and C-CDs. (b) The corresponding emission spectra of N-CDs at different excitation wavelengths from 300 to 360 nm; (Insets) photographs showing the colour change of N-CDs solution from yellow to blue after excitation under a UV lamp at 365 nm. (c) Emission spectra of C-CDs on varying the excitation wavelength. (d) Time-resolved fluorescence decay spectra of N-CDs and C-CDs.

when the excitation wavelength was changed in the range of 300–360 nm with 10 nm increments. The fluorescence intensity of N-CDs depended on the excitation wavelength, as shown in Fig. 2b. It was noticed that the fluorescence intensity of N-CDs increased and then decreased with the increment of the excitation wavelength. In comparison, the strongest emission intensity of C-CDs was observed at 435 nm on varying the excitation wavelength from 320 to 390 nm (Fig. 2c).

Subsequently, the fluorescence lifetimes (τ) of N-CDs and C-CDs were investigated by time-resolved fluorescence by employing the time-correlated single-photon counting (TCSPC) technique (excitation wavelength at 370 nm). The decay curves of both CDs were fitted using biexponential functions. The decay time of N-CDs was measured as about 5.69 ns, which had two components: 2.35 ns (*ca.* 43.8%) and 8.52 ns (*ca.* 56.2%) (Fig. 2d). Meanwhile, the average lifetime of C-CDs was calculated to be 5.01 ns.

3.3 Selective and sensitive detection of I⁻

Considering the adaptive property of luminescent materials and the simultaneous great change in fluorescence, we have investigated the potential use of the prepared N-CDs as an environment-responsive fluorescent probe. To explore the application of the as-prepared N-CDs in halide-ion sensing, four halide ions (F⁻, Cl⁻, Br⁻, and I⁻) were added to the aqueous solution of fluorescent N-CDs, respectively, and the emission response of the fluorescent probe was captured, as shown in Fig. 3a. The performed fluorescence study indicated that I⁻ had

the greatest effect of fluorescence (FL) quenching among all the tested ions, while F⁻ and Cl⁻ had only a slight FL quenching effect. In the presence of Br⁻, the fluorescence quenching of N-CDs was not as obvious as in the presence of I⁻. Furthermore, the lifetime of N-CDs after the addition of different halide ions (9.56 mM) was measured by the TCSPC technique. The average lifetime of N-CDs decreased to 5.61 ns, 5.39 ns, 4.86 ns and 2.20 ns with the addition of F⁻, Cl⁻, Br⁻, and I⁻, respectively, confirming that only I⁻ had a dramatic effect on the FL decay pathway of N-CDs (Fig. 3b). These phenomena demonstrated the high selectivity of the fluorescent probe for the detection of I⁻, which can be attributed to the special coordination interaction between I⁻ and the amino- and amide groups of N-CDs in contrast to the existence of only weak interactions between the N-CDs and other halide ions.

In order to evaluate the sensitivity of N-CDs, various concentrations of I⁻ (from 12.5 μM to 9.56 mM) were studied by means of fluorescence titration. The fluorescence intensity of N-CDs declined sharply first and decreased gradually at the later stage with the stepwise addition of I⁻ under excitation at 320 nm (Fig. 3c). When the concentration of I⁻ was 887 μM, the fluorescence quenching degree of N-CDs was more than 50%. In addition, the quenching efficiency was analyzed by employing the Stern–Volmer equation, $F_0/F = 1 + K_{sv}[I^-]$, where K_{sv} is the quenching constant, $[I^-]$ is the concentration of I⁻, and F_0 and F represent the fluorescence emission intensities at 408 nm when I⁻ is absent and present, respectively (Fig. S3, ESI†).[39] As shown in Fig. 3d, the relationship showed good linearity from 12.5 to
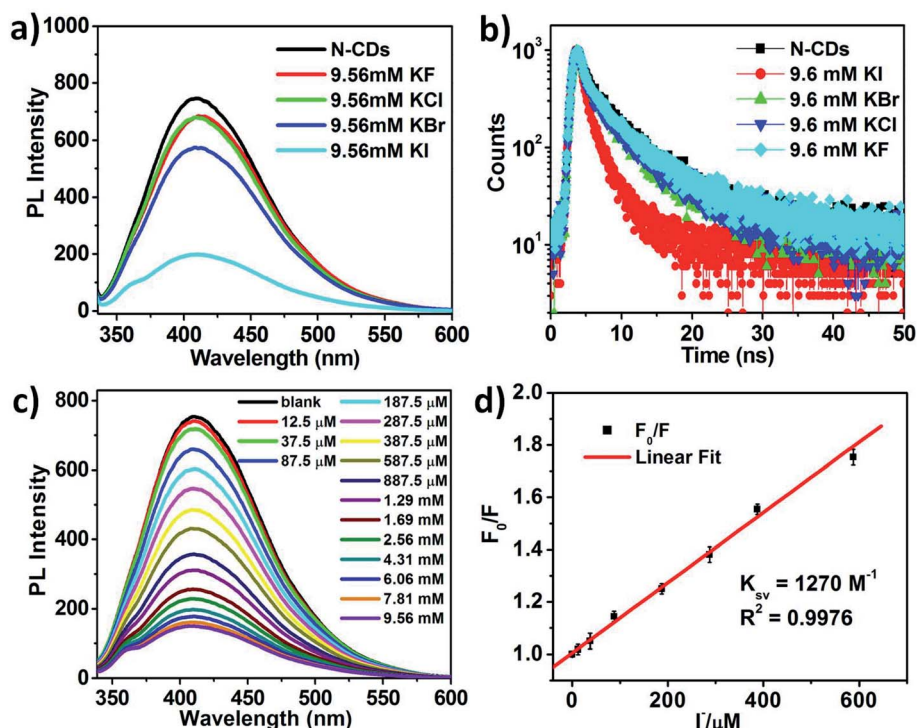
Fig. 3 (a) Comparison of the fluorescence intensities of N-CDs (50 μg.mL⁻¹) upon the addition of different halide ions (9.56 mM). (b) Time-resolved fluorescence decay spectra of N-CDs in response to different halide ions. (c) The fluorescence titration of the N-CDs in the presence of I⁻ ions (0 to 9.56 mM). (d) The linear relationship between F_0/F and I⁻ concentration (from 12.5 to 587 μM).

587 μM. Meanwhile, the K_{sv} value was determined to be 1270 M^{-1}, and the limit of detection (LOD) was calculated to be 0.47 μM based on the signal/noise ratio of 3.[40] Consequently, the results demonstrate that the N-CDs are highly sensitive fluorescent probes for iodide sensing and have a wide linear range.

3.4 Investigation of the FL-quenching mechanism

In order to investigate the FL-quenching mechanism of N-CDs induced by I⁻, the UV-vis absorption spectra and fluorescence spectra were analyzed. Fig. 4a shows that there was no obvious overlap between the absorption spectrum of KI and the excitation spectrum of N-CDs, which indicates that the exciting light was not absorbed by I⁻, thereby eliminating the possibility of

direct fluorescence quenching of N-CDs.[41] This result demonstrated that the FL-quenching process of N-CDs did not occur *via* the inner filter effect. Meanwhile, the absorption peak (275 nm) of N-CDs disappeared after the addition of KI (9.6 mM), suggesting the formation of stable excited complexes between N-CDs and I⁻ (Fig. 4b).

To get further insights into the PL quenching mechanism, the molecular geometry and Gibbs free energies of N-CDs and N-CDs/I⁻ in water (298.15 K) were determined by Density Functional Theory (DFT) calculations at the bp86/6-31G (d) level. Based on the main component cotton, amino-substituted pyrone structures have been proposed as the chromophore units of N-CDs. The optimized molecular geometry of
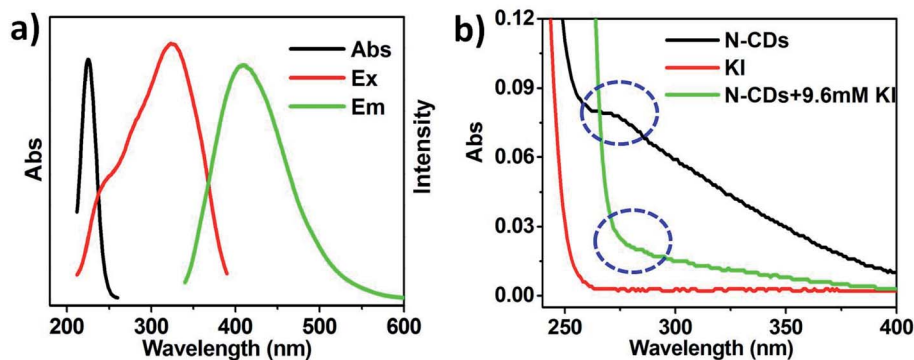

Fig. 4 (a) Absorption of I⁻ and the excitation and emission bands of N-CDs. (b) UV-vis absorption of N-CDs, KI and N-CDs/I⁻.

a) E_{gap} = 2.39 eV

b) E_{gap} = 2.36 eV

3.20 Å

3.07 Å

3.12 Å

ΔG = -23.63 kJ/mol

● C   ○ H   ● O   ● N   ● I⁻

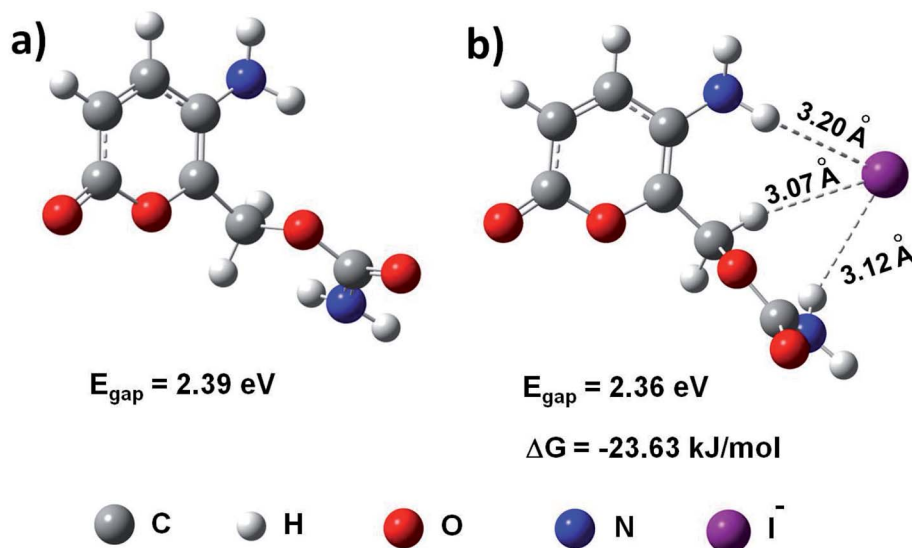**Fig. 5** (a) The optimized molecular geometry of the chromophore unit of N-CDs. (b) The optimized molecular geometry between N-CDs and I⁻.

a chromophore unit is shown in Fig. 5a. On the basis of the HOMO (−4.91 eV) and LUMO energies (−2.52 eV), the energy gap value (E_g) of the optimized geometries was 2.39 eV.

While N-CDs and I⁻ formed stable complexes (Fig. 5b), the distances between I⁻ and the H atoms of the amino (–NH₂), methylene (–CH₂) and amide (–C(=O)NH₂) groups of N-CDs were 3.20 Å, 3.07 Å and 3.12 Å respectively, indicating that multiple N–H···I⁻, C–H···I⁻ and C(=O)N–H···I⁻ interactions existed between the two moieties. As a result, the HOMO and LUMO energies of N-CDs changed to −4.85 eV and −2.49 eV, respectively, manifesting that the presence of I⁻ did not obviously affect the E_g (2.36 eV) of N-CDs. Meanwhile, the HOMO (−0.22 eV) and LUMO (0.0399 eV) energy levels of I⁻ were calculated, which were both much higher than the E_{LUMO} (−2.49 eV) of N-CDs, indicating that the electron transfer process from N-CDs to I⁻ was hardly taking place.[42]

Furthermore, the relative Gibbs free energies (ΔG) of N-CDs, I⁻ and N-CDs/I⁻ in water (298.15 K) were computed at the bp86/6-31G (d) level. Subsequently, the corresponding binding energy of N-CDs/I⁻ was found to be −23.63 kJ mol⁻¹, while the relative binding energy of C-CDs/I⁻ was −13.64 kJ mol⁻¹, which is much lower than that of N-CDs/I⁻ (Fig. S4 and Table S2, ESI†).[35,43] These results clearly demonstrate that the amino- and amide groups play a significant role in iodide recognition. Therefore, the chromophore units of N-CDs gather closer and closer with the addition of I⁻, giving an appropriate distance for π–π stacking between the chromophore units.[44] Moreover, the TEM experiment also confirmed the aggregation process when I⁻ was added to the N-CDs solution. The result showed spherical morphology with diameters in the range from 5 to 12 nm, convincingly indicating the formation of N-CDs/I⁻/N-CDs aggregates (Fig. 6a). The exciplexes generated through π–π interactions dissipated the excited energy, thereby leading to a large non-radiative transition.

The PL quenching mechanism was further verified through the time-resolved fluorescence decay spectra, which were used to study the excitation behavior of N-CDs when the I⁻ ions were absent and present (Fig. 6b). The emission of blank N-CDs

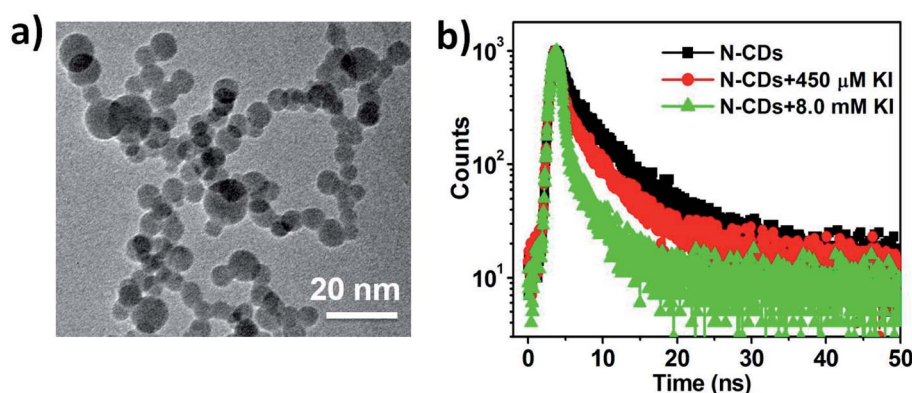**Fig. 6** (a) TEM image of N-CDs upon the addition of I⁻ (9.0 mM). (b) Time-resolved peak fluorescence of N-CDs (50 μg mL⁻¹) in response to different I⁻ concentrations.

Table 1 Fluorescence decay rates of N-CDs in the absence and presence of different I⁻ concentrations

	C_{I^-} (mM)	$\Phi_{FL}{}^a$	τ (ns)	k_r (s⁻¹)	k_{nr} (s⁻¹)
N-CDs	0	18.79%	5.69	3.30×10^7	1.40×10^8
N-CDs/I⁻	0.45	12.36%	4.31	2.86×10^7	2.04×10^8
N-CDs/I⁻	8.0	5.26%	2.70	1.95×10^7	3.58×10^8

^{a} Φ_{FL} values were estimated on the basis of the slope method (Fig. S5, see ESI).

showed biexponential decay with an average lifetime of $\tau = 5.69$ ns ($\Phi_F = 18.79\%$). Meanwhile, the initial radiative decay rate (k_r) and non-radiative decay rate (k_{nr}) were approximately determined to be 3.30×10^7 s⁻¹ and 1.40×10^8 s⁻¹ respectively, since Φ_F equals the product of τ and k_r. After coordination with I⁻ ions (450 μM), the average lifetime of N-CDs changed to 4.31 ns ($\Phi_F = 12.36\%$) and the radiative decay rate (k_r) declined to be 2.86×10^7 s⁻¹. When the concentration of I⁻ was 8.0 mM, the average lifetime value of the N-CDs/I⁻ system decreased to 2.70 ns ($\Phi_F = 5.26\%$), yielding a relatively lower radiative decay rate ($k_r = 1.95 \times 10^7$ s⁻¹) and a much higher non-radiative decay rate ($k_{nr} = 3.50 \times 10^8$ s⁻¹) compared with those of blank N-CDs (Table 1). In comparison, the average lifetime of C-CDs changed from 5.01 ns to 3.81 ns after the addition of I⁻ (8.0 mM) on fitting the data (Fig. S6, ESI†).

At the molecular level, the intermolecular interactions and intramolecular effects would greatly affect the emission intensity of the chromophore units.[45] As for the N-CDs/I⁻ solution, the multiple N–H⋯I⁻, C–H⋯I⁻ and C(=O)N–H⋯I⁻ interactions between the amino-/amide groups of N-CDs and I⁻ would facilitate π–π stacking between different chromophore units and restrain the radiative recombination of the excitons, resulting in a high non-radiative decay rate and shortened lifetime. The significantly reduced lifetime demonstrated that the excited energy dissipation by exciplexes led to the dynamic quenching process.

3.5 Detection of I⁻ in tap water

As iodide is an important trace element in the human body and intracellular environment, the N-CD-based fluorescent switch was applied for the detection of I⁻ in tap water. Considering the presence of residual hypochlorite, tap water was pretreated by exposing it to sunlight and heat in order to eliminate possible hypochlorite interference. The concentration of I⁻ in tap water was determined to be 2.1 μM according to the Stern–Volmer

Table 2 Detection of iodide ion in tap water

Sample	Addition (μM)	Measured (μM)	Recovery (%)	RSD (%)
1	0	2.1	—	2.2
2	4	6.2	103	1.8
3	20	23.4	106	3.0
4	60	60.8	98.0	2.8
5	100	97.1	95.1	2.7

equation. As shown in Table 2, I⁻ ion recovery in tap water ranged from 95.1% to 106%, indicating the reliability, fast response and detection accuracy of the method. Due to the convenience and practicality of this method, there is more scope for developing sensing materials for the selective and sensitive detection of halide ions.

4. Conclusions

In summary, a promising fluorescent sensing material was prepared by a hydrothermal method by employing cotton as the natural carbon source and urea as the nitrogen source. The as-prepared N-CDs were characterized through a combination of TEM, UV-vis absorption, FTIR, fluorescence spectroscopy and fluorescence lifetime measurements. Importantly, the fluorescent N-CDs were used for the selective and sensitive detection of I⁻ in a wide linear range from 12.5 μM to 587 μM, and the lowest detection limit was estimated to be 0.47 μM based on the quenching effect with the addition of I⁻. Moreover, UV-vis/fluorescence spectroscopy, DFT calculations, TEM and time-resolved fluorescence decay measurements were employed to investigate the quenching mechanism by analyzing the excitation behavior of the aqueous N-CDs solution in the absence and presence of I⁻. The reduced lifetime demonstrated that dissipation of excited energy resulted in the dynamic quenching process. Due to the facile production and stable fluorescence properties, fluorescent N-CDs are expected to have many potential applications in sensing, catalysis, optical device and medical areas.

Conflicts of interest

There are no conflicts to declare.

Acknowledgements

References

1 I. L. Lee, Y.-M. Sung, C.-H. Wu and S.-P. Wu, *Microchim. Acta*, 2014, **181**, 573–579.

2 J. A. Bishop, G. Wu, R. P. Tufano and W. H. Westra, *Thyroid*, 2012, **22**, 690–694.

3 Y. Wu, W. Chen, J. Shen, L. Tan, M. R. L'Abbe, E. N. Pearce, W. Wang, X. Tian, W. Wang and W. Zhang, *Nutr. Res.*, 2018, **55**, 72–80.

4 C. Tuccilli, E. Baldini, E. Truppa, B. D'Auria, D. De Quattro, G. Cacciola, T. Aceti, G. Cirillo, A. Faiola, P. Indigeno, L. D'Aliesio, F. Gazzellone, M. Bononi, E. D'Armiento,

G. Carbotta, D. Pironi, A. Catania, S. Sorrenti and S. Ulisse, *Nutrition*, 2018, **50**, 60–65.

5 Y. Zhang, W. Zhao, Y. Zhao, Y. Mao, T. Su, Y. Zhong, S. Wang, R. Zhai, J. Cheng, X. Fang, J. Zhu and H. Yang, *J. Proteome Res.*, 2020, **19**, 2539–2552.

6 M. Kaykhaii and M. Sargazi, *Spectrochim. Acta, Part A*, 2014, **121**, 173–179.

7 E. Espada-Bellido, Z. Bi, P. Salaün and C. M. G. van den Berg, *Talanta*, 2017, **174**, 165–170.

8 A. Machado, R. B. R. Mesquita, S. Oliveira and A. A. Bordalo, *Talanta*, 2017, **167**, 688–694.

9 L. Rong, L. W. Lim and T. Takeuchi, *Microchem. J.*, 2013, **108**, 113–116.

10 J. Valdes-García, L. D. Rosales-Vázquez, I. J. Bazany-Rodríguez and A. Dorazco-González, *Chem.–Asian J.*, 2020, **15**, 2925–2938.

11 D. Y. Lee, N. Singh, M. J. Kim and D. O. Jang, *Org. Lett.*, 2011, **13**, 3024–3027.

12 Z. Chen, R. Sun, S. Feng, D. Wang and H. Liu, *ACS Appl. Mater. Interfaces*, 2020, **12**, 11104–11114.

13 A. Niaz, A. Bibi, Huma, M. I. Zaman, M. Khan and A. Rahim, *J. Mol. Liq.*, 2018, **249**, 1047–1051.

14 J. Song, L. Zhao, Y. Wang, Y. Xue, Y. Deng, X. Zhao and Q. Li, *Nanomaterials*, 2018, **8**, 1043.

15 M. K. Salomón-Flores, C. L. Hernández-Juárez, I. J. Bazany-Rodríguez, J. Barroso-Flores, D. Martínez-Otero, R. López-Arteaga, J. Valdés-Martínez and A. Dorazco-González, *Sens. Actuators, B*, 2019, **281**, 462–470.

16 B. Zhang, Y. He and Z. Fan, *J. Photochem. Photobiol., A*, 2018, **367**, 452–457.

17 J. Zhang, Y. Li and S. Han, *Microchem. J.*, 2019, **147**, 1141–1146.

18 C. Hu, M. Li, J. Qiu and Y.-P. Sun, *Chem. Soc. Rev.*, 2019, **48**, 2315–2337.

19 X. Wei, J. Yang, L. Hu, Y. Cao, J. Lai, F. Cao, J. Gu and X. Cao, *J. Mater. Chem. C*, 2021, **9**, 4425–4443.

20 Indriyati, I. Primadona, F. A. Permatasari, M. A. Irham, M. Nasir and F. Iskandar, *Nanoscale*, 2021, **13**, 7523–7532.

21 L. Ai, Y. Yang, B. Wang, J. Chang, Z. Tang, B. Yang and S. Lu, *Sci. Bull.*, 2021, **66**, 839–856.

22 Y. Liu, H. Huang, W. Cao, B. Mao, Y. Liu and Z. Kang, *Mater. Chem. Front.*, 2020, **4**, 1586–1613.

23 S. Lu, L. Sui, J. Liu, S. Zhu, A. Chen, M. Jin and B. Yang, *Adv. Mater.*, 2017, **29**, 1603443.

24 B. Wang, J. Li, Z. Tang, B. Yang and S. Lu, *Sci. Bull.*, 2019, **64**, 1285–1292.

25 W. Li, Y. Liu, B. Wang, H. Song, Z. Liu, S. Lu and B. Yang, *Chin. Chem. Lett.*, 2019, **30**, 2323–2327.

26 W. Meng, X. Bai, B. Wang, Z. Liu, S. Lu and B. Yang, *Energy Environ. Mater.*, 2019, **2**, 172–192.

27 S. Zhu, Q. Meng, L. Wang, J. Zhang, Y. Song, H. Jin, K. Zhang, H. Sun, H. Wang and B. Yang, *Angew. Chem., Int. Ed.*, 2013, **52**, 3953–3957.

28 S. Liu, Y. He, Y. Liu, S. Wang, Y. Jian, B. Li and C. Xu, *Chem. Commun.*, 2021, **57**, 3680–3683.

29 C. Han, Z. Cui, Z. Zou, Sabahaiti, D. Tian and H. Li, *Photochem. Photobiol. Sci.*, 2010, **9**, 1269–1273.

30 H. Li, C. Han and L. Zhang, *J. Mater. Chem.*, 2008, **18**, 4543–4548.

31 A. O. Aswathy, S. M. Anju, J. Jayakrishna, N. S. Vijila, J. S. Anjali Devi, B. Anjitha and S. George, *J. Fluoresc.*, 2020, **30**, 1337–1344.

32 Z. Cao, W. Zhang, X. Ning, B. Wang, Y. Liu and Q. X. Li, *J. Agric. Food Chem.*, 2017, **65**, 10115–10122.

33 S. Nam, M. B. Hillyer, B. D. Condon, J. S. Lum, M. N. Richards and Q. Zhang, *J. Agric. Food Chem.*, 2020, **68**, 13231–13240.

34 X. Wen, L. Shi, G. Wen, Y. Li, C. Dong, J. Yang and S. Shuang, *Sens. Actuators, B*, 2015, **221**, 769–776.

35 Y. Hu, J. Yang, L. Jia and J.-S. Yu, *Carbon*, 2015, **93**, 999–1007.

36 Q. Huang, Q. Li, Y. Chen, L. Tong, X. Lin, J. Zhu and Q. Tong, *Sens. Actuators, B*, 2018, **276**, 82–88.

37 X.-W. Hua, Y.-W. Bao and F.-G. Wu, *ACS Appl. Mater. Interfaces*, 2018, **10**, 10664–10677.

38 H. Nie, M. Li, Q. Li, S. Liang, Y. Tan, L. Sheng, W. Shi and S. X.-A. Zhang, *Chem. Mater.*, 2014, **26**, 3104–3112.

39 G. Gao, Y.-W. Jiang, H.-R. Jia, J. Yang and F.-G. Wu, *Carbon*, 2018, **134**, 232–243.

40 T.-T. Xu, J.-X. Yang, J.-M. Song, J.-S. Chen, H.-L. Niu, C.-J. Mao, S.-Y. Zhang and Y.-H. Shen, *Sens. Actuators, B*, 2017, **243**, 863–872.

41 M. Wang, Y. Wan, K. Zhang, Q. Fu, L. Wang, J. Zeng, Z. Xia and D. Gao, *Anal. Bioanal. Chem.*, 2019, **411**, 2715–2727.

42 B. Ju, Y. Wang, Y.-M. Zhang, T. Zhang, Z. Liu, M. Li and S. Xiao-An Zhang, *ACS Appl. Mater. Interfaces*, 2018, **10**, 13040–13047.

43 C. Geng, S. Zhang, C. Duan, T. Lu, R. Zhu and C. Liu, *RSC Adv.*, 2015, **5**, 80048–80056.

44 X. Ji, Y. Yao, J. Li, X. Yan and F. Huang, *J. Am. Chem. Soc.*, 2013, **135**, 74–77.

45 J. Zhang, B. Xu, J. Chen, L. Wang and W. Tian, *J. Phys. Chem. C*, 2013, **117**, 23117–23125.